IEEE Photonics Journal
An IEEE Photonics Society Publication

Asymmetric all Silicon Micro-Antenna Array for High Angle Beam Bending in Terahertz Band

Volume 11, Number 2, April 2019

Zihao Liu
Xiangjun Li
Jie Yin
Zhi Hong

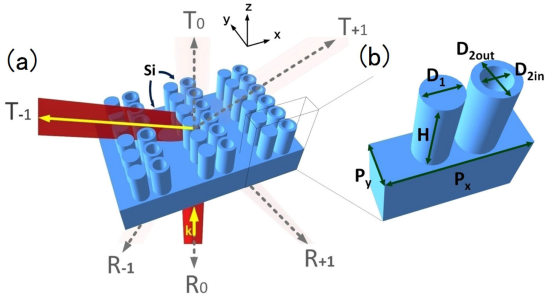

DOI: 10.1109/JPHOT.2019.2901307
1943-0655 © 2019 IEEE

Asymmetric all Silicon Micro-Antenna Array for High Angle Beam Bending in Terahertz Band

Zihao Liu,[1,2] **Xiangjun Li,**[1,2] **Jie Yin,**[1,2] **and Zhi Hong**[1]

[1]Centre for THz Research, China Jiliang University, Hangzhou 310018, China
[2]College of Information Engineering, China Jiliang University, Hangzhou 310018, China

DOI:10.1109/JPHOT.2019.2901307

Manuscript received November 22, 2018; revised February 5, 2019; accepted February 11, 2019. Date of publication March 4, 2019; date of current version March 18, 2019. This work was supported by the National Natural Science Foundation of China under Grants 61875179 and 61875251. Corresponding author: Xiangjun Li (e-mail: Xiangjun_li@cjlu.edu.cn).

Abstract: Phase mapping of metasurfaces with a finite number of elements is popular in wavefront manipulation. However, in high angle beam bending, the efficiency of bending beams drastically drops, which will greatly limit the applications of metasurface in photonic devices. Here, we propose an all silicon asymmetric dimer micro-antenna array used as meta-grating to achieve large bending angle and high efficiency for both P- and S- polarized incident wave at 0.3 THz. The geometric structure of the dimer consisting of one solid and one hollow pillar was meticulously optimized to realize a large bending angle of 70.2° with the diffraction efficiency of 73.1% and 37.8% for the P- and S- polarizations, respectively. The proposed all silicon metasurface can be easily prepared with CMOS technology, and can be used in flat lenses with high numerical aperture or other photonic devices in THz range.

Index Terms: All-dielectric metasurface, micro-antenna array, beam bending.

1. Introduction

Metasurfaces, which are generally composed of sub-wavelength scatters patterned on planar interfaces, can exert a specific phase, polarization, amplitude field distribution of the transmitted or reflected electromagnetic wave in sub-wavelength scale, leading to plenty planar device applications including absorber, beam bending, polarization control, holograms, wave plates, vortex, Bessel, or vector beam generations, and flat lens, etc [1]–[12]. Metasurfaces have emerged a great potential to replace bulky optical devices due to their ultra-thin and planar features with strong beam bending abilities. Meanwhile, the controlling strategy is universal and applies to a broad spectral range, including terahertz with its unique properties including nonionizing photon energy, spectral fingerprinting of molecular vibrations, and high transparency of some optically opaque materials finding it highly promising applications in chemical identification [13], material characterization [14], biological sensing [15], and medical imaging [16]. One of the popular methods to realize such wavefront control of continuous linear phase distribution is discretized with periodically repeated particle chains providing the appropriate phase accumulation, called phase mapping [9]–[12]. Due to the strong Ohmic losses and large reflections, it is hard for plasmonic metasurfaces to realize high transmissions [17]–[19], e. g., low focusing efficiency of around 10% for single layer [12] and

30% for bilayer metalens [20]. Using high refractive index dielectrics as particles instead of metallic ones can effectively overcome these challenges [21]–[27], and a high efficiency of 86% can be reached with NA = 0.8 [28]. However, such phase mapping method with a finite number of elements in a unit cell designed for large angle bending will encounter a drastic drop of the efficiency [29]. For example, the collection angle of 76° corresponding to NA = 0.97 have been reported for a dielectric metalens, but the efficiency droped to only 42% [23]. The alternative solution is using impedance profiling with the exact boundary conditions, but it will introduce locally active or strongly non-local passive metasurfaces with high fabrication resolution [30]–[33], thus it is difficult to be applied in metalens because there is no explicit relationship between the surface impedance and bending angle. There are also pioneer metagrating works circumventing phase mapping method to continuously modulate the phase, channelling incident light into a specific diffraction order, although they are performed in the reflection plasmonic platform, such as metagrating with subwavelength metallic slit array and metallic nano-groove gratings [34]–[36]. Moreover, in the visible-near-infrared regime, several research results have shown that the phase and amplitude of the polarized incident beam can be changed by changing the distance between meta-atoms in the arrays or by adjusting the displacement and direction angles of multiple nanorods in one unit cell other than the geometric parameters [37]–[39]. Recently, metasurfaces by arranging asymmetric dielectric nanoantennas as diffractive gratings can circumvent the above difficulties [40]–[42]. It directly controls the wave energy distribution by diffraction gratings and does not rely on phase/amplitude mapping, where scattering directivity patterns of the each unit cell allows suppression or enhancement of selected diffraction orders desirably to channel the incident wave energy into one particular diffraction order in transmission or reflection causing specific beam bending. A.I. Kuznetsov *et. al.* [42] proposed an asymmetric nanoantenna array for a metalens working at 715nm, where the dimer structure of the meta-grating consists of two silicon pillars with different diameter, and high bending angle of 82° with transmission of 40% (15%) for P- (S-) polarized incident light was achieved. In this paper, we propose an asymmetric dimer micro-antenna array consisting of one solid and one hollow silicon pillar as meta-grating on silicon substrate for THz beam bending. We optimized the structure of the planar meta-grating to achieve large beam bending angle and high efficiency at 0.3 THz. The bending angle reaches 70.2° with the efficiency of 73.1% and 37.8% for the P- and S- polarized incident wave, respectively. As comparison, the efficiency for the P-polarized light drops to 62.5% at the same bending angle for a silicon two-pillar dimer structure. We can control the diffraction angle by changing the period of the diffraction unit. The larger period corresponds to a smaller deflection angle which shows the same characteristics as grating. We can optimize the structure at different diffraction periods to achieve a wide range of bending angles. The proposed all silicon metasurface is ease fabrication at present CMOS process, and can be used to design flat lenses with high numerical aperture and efficiency or other photonic devices in THz range.

2. Designs and Results

The asymmetric dimer micro-antennas have been previously proven to generate asymmetric radiation patterns in which the interacting particles become a 'perfect' deflecting a normally incident wave into a single diffractive order without transmission or reflection to other diffractive orders (Fig. 1(a)). Fig. 1(b) shows our proposed unit cell of an array designed to bend normally incident 0.3 THz planar wave at an angle of 70.2°. It consists of an asymmetric dimer micro-antennas made of one solid and one hollow silicon (Si) pillar of height H = 530 μm placed on top of Si substrate and surrounded by air. The silicon has a high refractive index of 3.415 and is low loss in terahertz band. The cylinder diameter is D_1 = 252 μm, and the inner and outer diameters of the hollow pillar are D_{2in} = 188 μm and D_{2out} = 284 μm, respectively. The gap between the two particles is G = 50 μm. The diffractive and non-diffractive periods of the square lattice are P_x = 1025 μm and P_y = 310 μm, respectively. The S- (P-) polarization is defined as the magnetic (electric) field directed along the axis of the dimer.

As seen from the Fig. 2, the energy is mainly channeled into the T_{-1} order tilted at 70.2° with respect to its normal incident with minimal distortion. The simulated transmission efficiencies

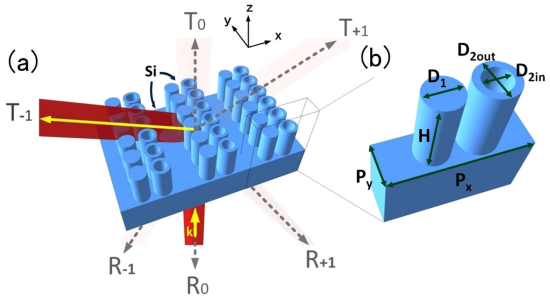

Fig. 1. (a) Schematic description of the controlled energy distribution among the supported diffraction orders determined by the diffractive period of the array, producing energy concentration into the T_{-1} diffraction order leading to THz beam bending at 70.2° when normally incident from the substrate side. (b) Unit cell of an array made of a silicon pillar and hollow pillar of height H = 530 μm on Si substrate and surrounded by air with $D_1 = 252$ μm, $D_{2in} = 188$ μm, $D_{2out} = 284$ μm, G = 50 μm, Px = 1025 μm, and Py = 310 μm.

into the different orders together with the total transmission, total reflection and transmission plus reflection are illustrated in Fig. 2(a) and 2(b) for P- and S-polarized wave at the operating frequency of 0.3 THz. The transmission spectrum demonstrates most of the P-polarized is channeled into the desired T_{-1} order reaching an efficiency of 73.1% with respect to the incident power. For the S-polarized wave the diffraction efficiency is smaller, reaching an efficiency of 37.8%. Fig. 2(c) and 2(d) shows a calculated far-field diagram at 0.3 THz for P- and S-polarized wave. It indicates a strong directivity towards the target direction, where the energy scattered into the other diffraction orders not only in transmission but also in reflection (indicated by the dashed line), is significantly suppressed. Fig. 2(e) and 2(f) illustrate the simulated normalized far-field intensity distribution on incident plane wave for different transmission diffraction orders when P- and S-polarized wave is incident. It describes the relationship of the corresponding diffraction angle and incident beam between 0.29 $\sim$ 0.34 THz. The three dashed lines are corresponding to the three main diffraction orders T_{-1}, T_0, T_{+1} supported in transmission, where the diffraction angle linearly decreases as frequency increases. Moreover, it is important to note that, the frequency of $\sim$0.326 THz, at which the far-field intensity is largest in the T_{-1} diffraction order, is not the one at the highest transmission of the T_{-1} diffraction order in Fig. 2(a)–2(b) (0.306 THz). This is because the full width at half maximum of T_{-1} distribution at 0.306 THz is larger than that at 0.326 THz. So there is a better balance between bending angle and transmission efficiency at 0.30 THz, which is very close to the highest transmission at 0.306 THz.

Figure 3(a) and 3(b) respectively show the FDTD simulated electric and magnetic field distributions when the micro-antenna array is illuminated by normally incident P-polarized plane wave at 0.3 THz. When the array is illuminated by S-polarized plane wave, simulated electric field and magnetic field distribution have been presented in Fig. 3(c) and 3(d). It reveals that energy is mainly concentrated into the designed order, and the diffraction angle is marked by the black solid lines. The color bars of the two electric and magnetic field maps are respectively the same so that it is convenient to compare the P- and S- polarized plane wave. This is evidenced by the plane wave emerging from the array tilted at 70.2° with respect to its normal with minimal distortion.

3. Discussion

Obviously the efficiency and bending angle in desired transmission diffraction order of the scattering unit are affected by many factors. Here, we discuss the influences of the scattering unit structure parameters, the dimer pattern and the property of the substrate material on the bending angle and efficiency.

Firstly, we scan the lengths of D_1, D_{2in}, G and H with the simulated normalized far-field intensity distribution on incident plane wave for different transmission diffraction orders under P- or S-

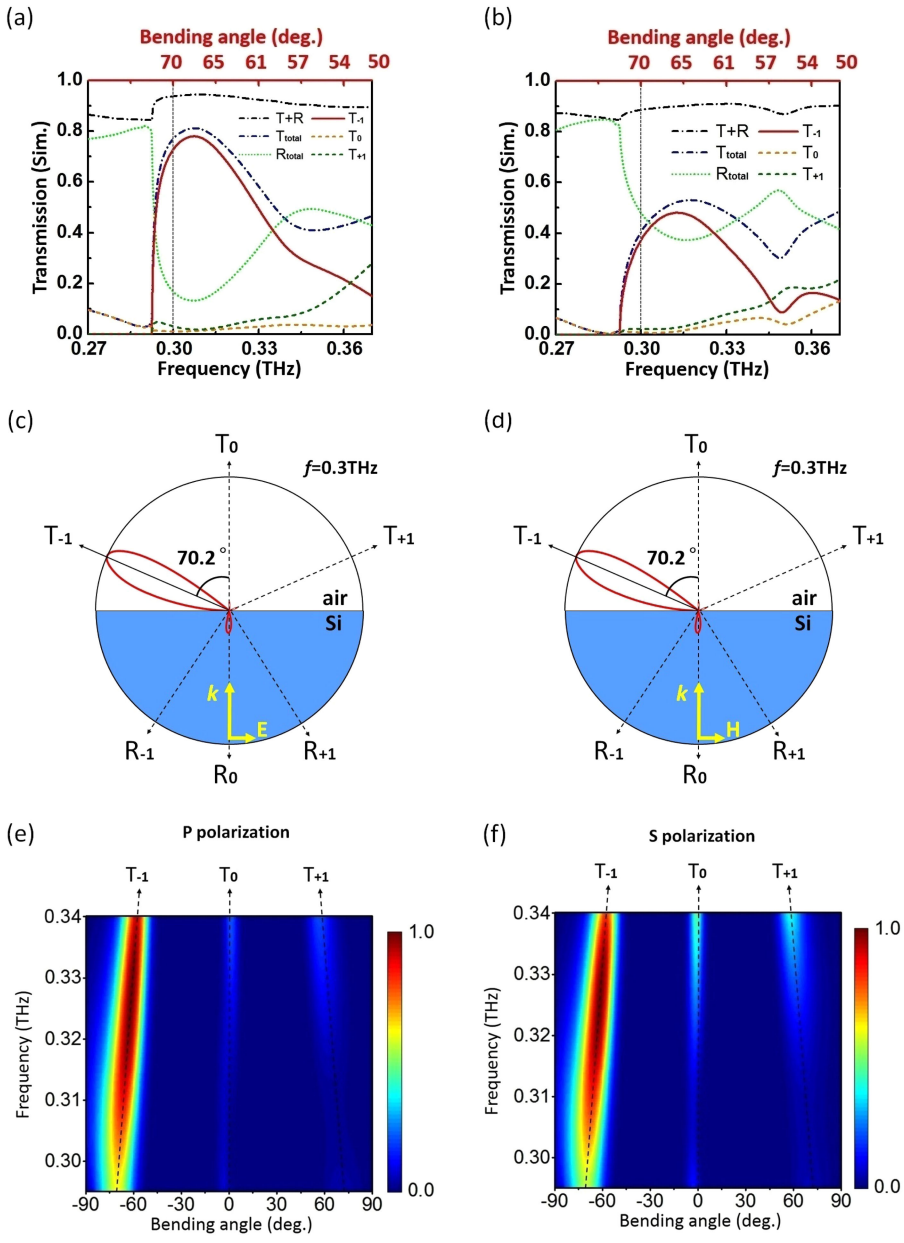

Fig. 2. (a) and (b) are simulated relations between frequency, transmission distribution and bending angle when (a) P- or (b) S-polarized wave is incident. Solid red line indicates desired transmission order (T_{-1}). T_0 and T_{+1} order are indicated by orange and olive dashed line. The total reflection, transmission, and transmission plus reflection are indicated by green dot, blue dash-dotted line, and black dash-dotted line. (c) and (d) are calculated far-field diagram of one dimer unit cell in the grating at 0.3 THz for (c) P- or (d) S-polarized wave. (e) and (f) are simulated normalized far-field intensity distribution on incident plane wave for three transmission diffraction orders as a function of the frequency and deflection bending angle when (e) P- or (f) S-polarized wave is incident.

polarized wave. The results are shown in Fig. 4, where the dashed lines correspond to the three diffraction orders supported in transmission. It is evident that if the parameters move away from the optimal positions (indicated by the red dashed line), the energy in the T_{-1} order will decrease while bending angle is not altered. The results reveal that geometry of dimers lay strong influences on coupling of inner resonance modes. Considering that it is hard to fabricate silicon pillars with different height, here we only discuss the dimer pillars with same height.

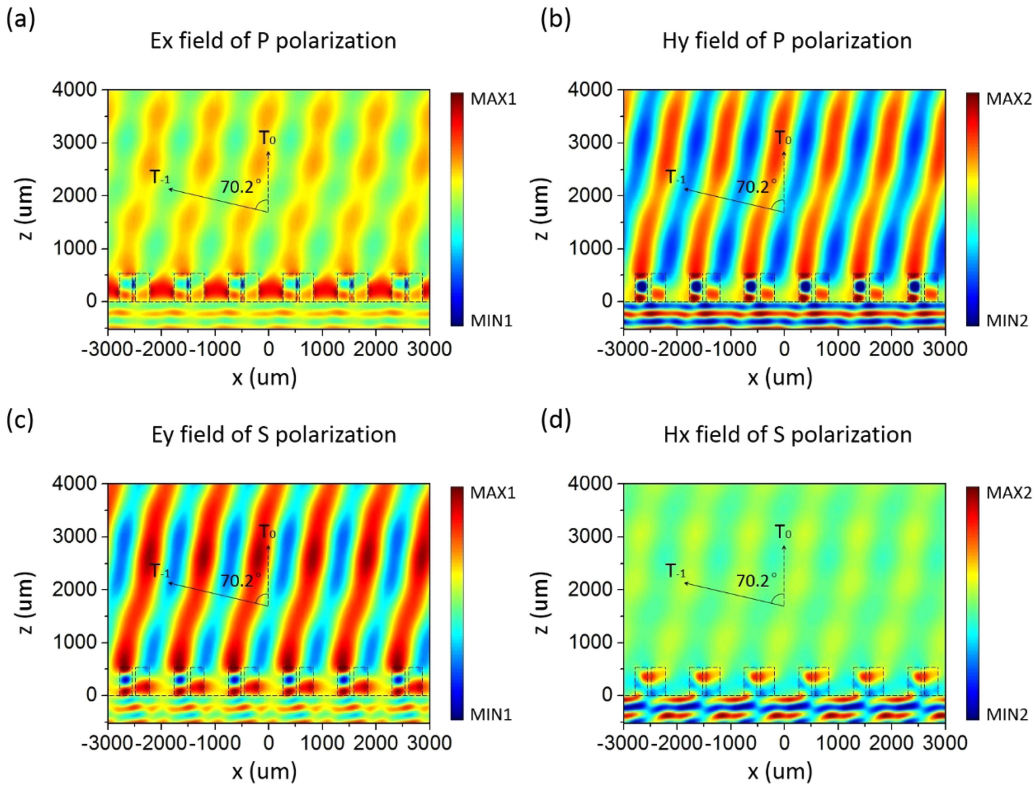

Fig. 3. FDTD simulated electric field [(a), and (c)] and magnetic field [(b), and (d)] distribution when the array is illuminated by P- or S- polarized plane wave normally incident at the operating frequency. The color bars of the two electric and magnetic field maps are respectively the same.

The optimization way we used here is single variable scanning strategy and optimizing parameters one by one for the ultimate highest efficiency. However, a better way is to use the multivariable optimization method, which is facing much larger calculation amount and higher requirements for physical hardware. It is one of limiting factors to achieve greater efficiency. We will try other effective multivariable optimization strategies and improving the efficiency in following work.

Secondly, the comparison of two different dimer structures is made to elucidate the privileges of our proposed profiles. We optimize the parameters of the dimer structure consisting of two solid silicon pillars with different diameter at frequency of 0.3 THz, and compare it to the dimer form of one solid and one hollow pillars. FDTD simulated results of transmission efficiencies of the designed diffraction order when the micro-antenna arrays are illuminated by P- or S-polarized wave are shown in Fig. 5. The transmission efficiency of the dimer which we have proposed (T_{-1} order) is 10% higher than that of the structure with two solid pillars when P-polarized wave is incident, but for S-polarized incident wave, the diffraction efficiency is almost equal at 0.3 THz.

At last we find out that it is necessary to minimize the energy lose caused by the reflection of the substrate. We use the silicon as substrate with large refractive index(∼3.415) in previous discussion, and in following we will try different substrates with lower refractive index, SiO_2(∼1.95) and Teflon(∼1.43) [43] to present their influences on transmission efficiency in the designed diffraction order. Fig. 6 demonstrates the T_{-1} transmission spectra with different substrates. Table 1 lists their transmission efficiencies under P- or S-polarized incident wave at 0.3 THz. It is noted that as the refractive index of the substrate decreases the transmission efficiency increases for P-polarized wave, but it doesn't change under S-polarized incident wave at the working frequency. The simulated results also indicate that the bending angle does not vary with different kinds of substrates.

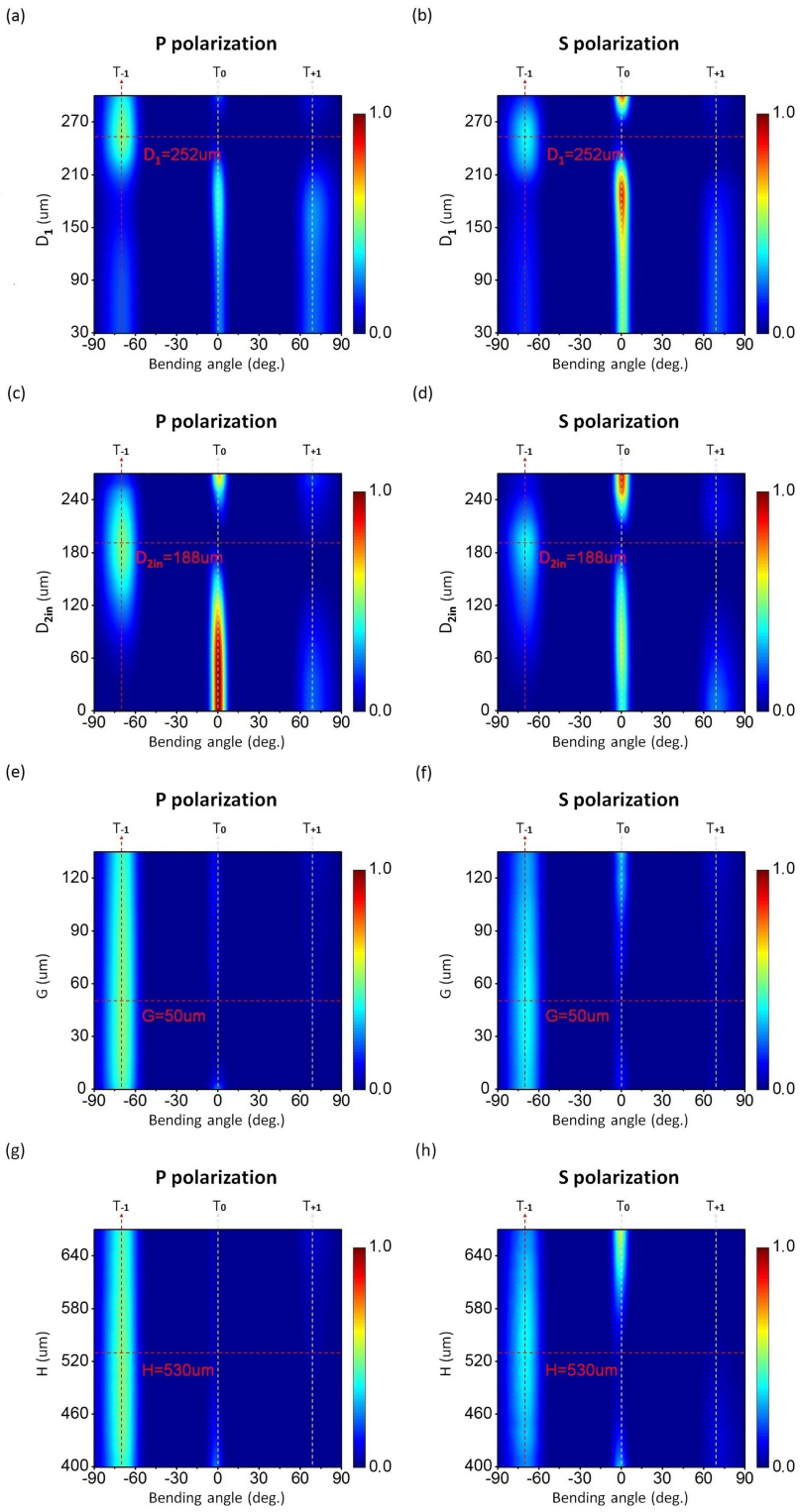

Fig. 4. Relations between different parameters (a) D_1, (c) D_{2in}, (e) G, (g) H and bending angle and energy in three transmission diffraction orders for P-polarized wave, [(b), (d), (f), and (h)] for S-polarized wave. Dashed lines with arrow indicate three diffraction orders. The color bars of the eight figures are the same. When scanning target parameter, others are at default sizes ($P_x = 1025\ \mu$m, $P_y = 310\ \mu$m, $D_1 = 252\ \mu$m, $D_{2out} = 284\ \mu$m, $D_{2in} = 188\ \mu$m, H = 530 μm, G = 50 μm).

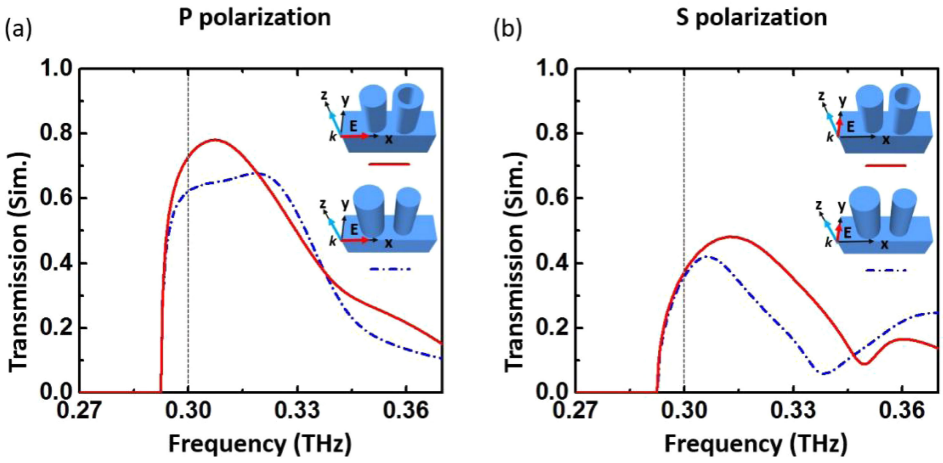

Fig. 5. Comparison of transmission distribution in the designed order of the dimer structure of one solid and one hollow pillar (red solid line) with the two solid pillars (blue dash-dotted line) under incident wave illumination with (a) P- and (b) S-polarization. Black dashed line indicates the designed operation frequency.

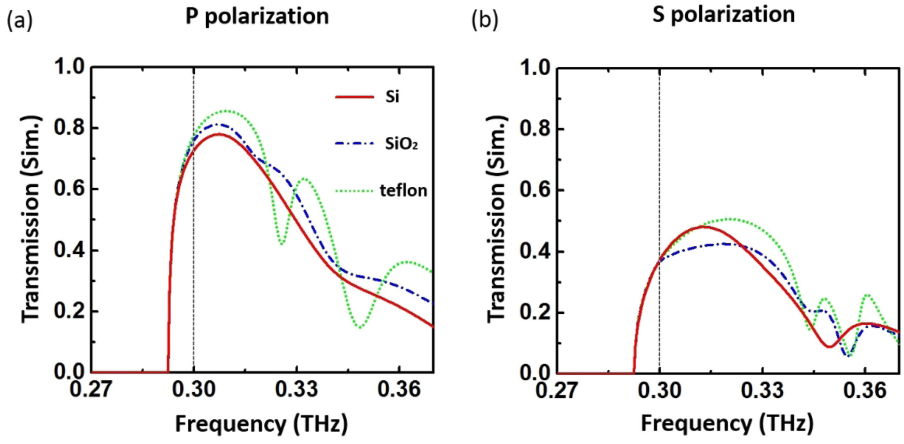

Fig. 6. Comparison of transmission in the designed order of the dimer with Si, SiO_2, and teflon substrates when (a) P- or (b) S-polarized wave is incident. Solid red line indicates structure with Si substrate. Green dotted line and blue dash-dotted line respectively indicates dimers with SiO_2 and teflon substrates.

TABLE 1
Transmission Efficiencies of the Array With 3 Different Substrates at 0.3 THz (Bending angle = 70.2°)

Substrate	Si	SiO_2	Teflon
P polarization	73.1%	76.4%	78.2%
S polarization	37.8%	37.1%	37.2%

The overall efficiency can be increased by using arrays with SiO_2 or Teflon substrate, however, it would increase fabrication cost and complexity, especially in terahertz range. Moreover, considering that the large reflection loss at the back surface (not shown in Fig. 1) due to the high refractive index of silicon can be cancelled by antireflection silicon pillar array [27], the proposed all silicon metasurface with CMOS compatible fabrication has great potential in terahertz compact functional devices.

4. Conclusion

We have proposed an asymmetric all silicon dimer micro-antenna array to control the scattering direction of the terahertz wave by optionally enhancing or suppressing the energy of the corresponding diffraction order. Comparing with the methods of the phase mapping with a finite number of elements and the impedance surface, the structure has the advantages of maintaining high efficiency in large angle bending and easy fabrication. We numerically demonstrate that the bending angle of our micro-antenna array reaches 70.2° with 73.1% (37.8%) efficiency on the incident P- (S-)polarized wave at operating frequency of 0.3THz. The affects of the geometry parameters, dimer pattern and different substrate materials are also discussed, while higher efficiency and larger bending angle might be obtained by multivariable optimizing methods, which will also face more difficulties and challenges. The proposed all silicon structure with CMOS compatible fabrication has a broad application in terahertz compact functional devices.

References

[1] N. Yu and F. Capasso, "Flat optics with designer metasurfaces," *Nat. Mater.*, vol. 13, no. 2, pp. 139–150, 2014.
[2] C. J. Changhasnain, P. Qiao, and W. Yang, "Recent advances in high-contrast metastructures, metasurfaces, and photonic crystals," *Adv. Opt. Photon.*, vol. 10, no. 1, pp. 180–245, 2018.
[3] M. Khorasaninejad and F. Capasso, "Metalenses: Versatile multifunctional photonic components," *Science*, vol. 358, no. 6367, 2017, Art. no. eaam8100.
[4] P. C. Wu *et al.*, "Versatile polarization generation with an aluminum plasmonic metasurface," *Nano Lett.*, vol. 17, no. 1, pp. 445–452, 2017.
[5] I. V. Shadrivov, K. Fan, W. J. Padilla, and X. Liu, "Experimental realization of a terahertz all-dielectric metasurface absorber," *Opt. Exp.*, vol. 25, no. 1, pp. 191–201, 2017.
[6] A. Arbabi, H. Yu, M. Bagheri, and A. Faraon, "Dielectric metasurfaces for complete control of phase and polarization with subwavelength spatial resolution and high transmission," *Nat. Nanotechnol.*, vol. 10, no. 11, pp. 937–943, 2015.
[7] L. Li, T. Li, X. M. Tang, S. M. Wang, Q. J. Wang, and S. N. Zhu, "Plasmonic polarization generator in well-routed beaming," *Light Sci. Appl.*, vol. 4, 2015, Art. no.e330.
[8] Z. Ma *et al.*, "Terahertz all-dielectric magnetic mirror metasurfaces," *ACS Photon.*, vol. 3, no. 6, pp. 1010–1018, 2016.
[9] F. Aieta *et al.*, "Aberration-free ultrathin flat lenses and axicons at telecom wavelengths based on plasmonic metasurfaces," *Nano Lett.*, vol. 12, no. 9, pp. 4932–4936, 2012.
[10] X. Chen *et al.*, "Dual-polarity plasmonic metalens for visible light," *Nat. Commun.*, vol. 3, 2012, Art. no. 1198.
[11] W. T. Chen *et al.*, "A broadband achromatic metalens for focusing and imaging in the visible," *Nat. Nanotechnol.*, vol. 13, no. 3, pp. 220–226, 2018.
[12] S. Wang *et al.*, "Broadband achromatic optical metasurface devices," *Nat. Commun.*, vol. 8, 2017, Art. no. 187.
[13] M. S. Islam *et al.*, "A novel approach for spectroscopic chemical identification using photonic crystal fiber in the terahertz regime," *IEEE Sensors J.*, vol. 18, no. 2, pp. 575–582, 2018.
[14] J. A. Hejase, E. J. Rothwell, and P. Chahal, "A multiple angle method for THz time-domain material characterization," *IEEE Trans. Terahertz Sci. Technol.*, vol. 3,no. 5, pp. 656–665, Sep. 2013.
[15] H. Yoshida *et al.*, "Terahertz sensing method for protein detection using a thin metallic mesh" *Appl. Phys. Lett.*, vol. 91, 2007. Art. no. 253901.
[16] Z. D. Taylor *et al.*, "THz medical imaging: In vivo hydration sensing," *IEEE Trans. Terahertz Sci. Technol.*, vol. 1, no. 1, pp. 201–219, Sep. 2011.
[17] A. Epstein and G. V. Eleftheriades, "Passive lossless huygens metasurfaces for conversion of arbitrary source field to directive radiation," *IEEE Trans. Antennas Propag.*, vol. 62, no. 11, pp. 5680–5695, Nov. 2014.
[18] K. Achouri and C. Caloz, "Design, concepts and applications of electromagnetic metasurfaces," *Nanophotonics*, vol. 7, no. 6, pp. 1095–1116, 2018.
[19] A. Epstein and G. V. Eleftheriades, "Huygens' metasurfaces via the equivalence principle: Design and applications," *J. Opt. Soc. Amer. B*, vol. 33, no. 2, pp. A31–A50, 2016.
[20] F. Qin *et al.*, "Hybrid bilayer plasmonic metasurface efficiently manipulates visible light," *Sci. Adv.*, vol. 2, no. 1, 2016, Art. no. e1501168.
[21] A. Y. Zhu, A. I. Kuznetsov, B. Luk'Yanchuk, N. Engheta, and P. Genevet, "Traditional and emerging materials for optical metasurfaces," *Nanophotonics.*, vol. 6, no. 2, pp. 452–471, 2017.
[22] A. I. Kuznetsov, A. E. Miroshnichenko, M. L. Brongersma, Y. S. Kivshar, and B. Luk'Yanchuk, "Optically resonant dielectric nanostructures," *Science*, vol. 354, no. 6314, 2016, Art. no. aag2472.
[23] A. Arbabi, H. Yu, A. J. Ball, M. Bagheri, and A. Faraon, "Subwavelength-thick lenses with high numerical apertures and large efficiency based on high-contrast transmitarrays," *Nat. Commun.*, vol. 6, 2015, Art. no. 7069.
[24] D. Jia *et al.*, "Transmissive terahertz metalens with full phase control based on a dielectric metasurface," *Opt. Lett.*, vol. 42, no. 21, pp. 4494–4497, 2017.
[25] D. Ruan *et al.*, "All-dielectric metalens for terahertz wave imaging," *Opt. Exp.*, vol. 26, no. 11, pp. 14132–14142, 2018.
[26] C. Ouyang *et al.*, "Polarization-independent all-silicon dielectric metasurfaces in the terahertz regime," *Photon. Res.*, vol. 6, no. 1, pp. 24–29, 2018.

[27] H. Zhang *et al*., "High-efficiency dielectric metasurfaces for polarization-dependent terahertz wavefront manipulation," *Adv. Opt. Mater.*, vol. 6, no. 1, 2018, Art. no. 1700773.
[28] M. Khorasaninejad, W. T. Chen, R. C. Devlin, J. Oh, A. Y. Zhu, and F. Capasso, "Metalenses at visible wavelengths: Diffraction-limited focusing and subwavelength resolution imaging," *Science*, vol. 352, no. 6290, pp. 1190–1194, 2016.
[29] Y. Ra'Di, D. L. Sounas, and A. Alù, "Metagratings: Beyond the limits of graded metasurfaces for wave front control," *Phys. Rev. Lett.*, vol. 119, no. 6, 2017, Art. no. 067404.
[30] S. A. Tretyakov, "Metasurfaces for general transformations of electromagnetic fields," *Philos. Trans. Roy. Soc. Mat. Phys. Eng. Sci.*, vol. 373, no. 2049, 2015, Art. no. 20140362.
[31] C. Pfeiffer and A. Grbic, "Metamaterial Huygens' surfaces: Tailoring wave fronts with reflectionless sheets," *Phys. Rev. Lett.*, vol. 110, no. 19, 2013, Art. no. 197401.
[32] N. M. Estakhri and A. Alù, "Wave-front transformation with gradient metasurfaces," *Phys. Rev. x*, vol. 6, no. 4, 2016, Art. no. 041008.
[33] A. Díaz-Rubio, V. S. Asadchy, A. Elsakka, and S. A. Tretyakov, "From the generalized reflection law to the realization of perfect anomalous reflectors," *Sci. Adv.*, vol. 3, no. 8, 2017, Art. no. e1602714.
[34] Z. L. Deng, Y. Y. Cao, X. P. Li, and G. P. Wang, "Multifunctional metasurface: From extraordinary optical transmission to extraordinary optical diffraction in a single structure," *Photon. Res.*, vol. 6, no. 5, pp. 443–450, 2018.
[35] Z. L. Deng, S. Zhang, and G. P. Wang, "Wide-angled off-axis achromatic metasurfaces for visible light," *Opt. Exp.*, vol. 24, no. 20, pp. 23118–23128, 2016.
[36] Z. L. Deng, S. Zhang, and G. P. Wang, "A facile grating approach towards broadband, wide-angle and high-efficiency holographic metasurfaces," *Nanoscale*, vol. 8, no. 3, pp. 1588–1594, 2016.
[37] Z. L. Deng *et al*., "Diatomic metasurface for vectorial holography," *Nano Lett.*, vol. 18, no. 5, pp. 2885–2892, 2018.
[38] Z. L. Deng *et al*., "Facile metagrating holograms with broadband and extreme angle tolerance" *Light: Sci. Appl.*, vol. 7, 2018, Art. no. 78.
[39] Z. L. Deng and G. X. Li, "Metasurface optical holography," *Mater. Today Phys.*, vol. 3, pp. 16–32, 2017.
[40] E. Khaidarov *et al*., "Asymmetric nanoantennas for ultra-high angle broadband visible light bending," *Nano Lett.*, vol. 17, no. 10, pp. 6267–6272, 2017.
[41] Z. Fan, M. R. Shcherbakov, M. Allen, J. Allen, and G. Shvets, "Perfect Diffraction with Bianisotropic Metagratings," 2018, arXiv: 1802.01269.
[42] R. Paniagua-Dominguez *et al*., "A metalens with near-unity numerical aperture," *Nano Lett.*,vol. 18, no. 3, pp. 2014–2132, 2018.
[43] J. R. Birch, J. D. Dromey, and J. Lesurf, "The optical constants of some common low-loss polymers between 4 and 40 cm^{-1}," *Infrared Phys.*, vol. 21, pp. 225–228, 1981.